https://doi.org/10.5194/acp-2022-321
Preprint. Discussion started: 18 May 2022

Atmospheric Chemistry and Physics Discussions

Measurement Report: A new coupled method of pH titration and size-resolved analysis to identify the structure, aging, and source of water-soluble organic carbon

Yuanyuan Qin[1], Juanjuan Qin[1,2], Xiaobo Wang[1], Kang Xiao[1], Ting Qi[1,6], Yuwei Gao[1], Xueming Zhou[5], Shaoxuan Shi[1], Jingnan Li[1], Jingsi Gao[3], Ziyin Zhang[4], Jihua Tan[1], Yang Zhang[1], and Rongzhi Chen[1]

[1] College of Resources and Environment, University of Chinese Academy of Sciences, Beijing, 100049, China
[2] Guangzhou Institute of Geochemistry, Chinese Academy of Sciences, Guangzhou, 510640, China
[3] School of Materials & Environmental Engineering, Shenzhen Polytechnic, Shenzhen, 518000, China
[4] Institute of Urban Meteorology, China Meteorological Administration, Beijing, 100089, China
[5] Faculty of Earth Resources, China University of Geosciences, Wuhan, 430074, China
[6] School of Chemical Sciences, University of Chinese Academy of Sciences, Beijing, 10049, China

Correspondence: Jihua Tan (tanjh@ucas.ac.cn) and Yang Zhang (zhangyang@ucas.ac.cn)

Abstract. Measuring water-soluble organic carbon (WSOC) in aerosols is critical, as WSOC is involved in many key particle-associated chemical reactions. Here, the coupled effects of pH and particle size on the chemical structures (functional groups) and optical properties (UV/fluorescence properties) of WSOC were investigated to explore the structure, aging, and source of these materials. The results showed that the specific UV absorbance at a wavelength of 254 nm ($SUVA_{254}$) and mass absorption efficiency (MAE_{365}) were higher in smaller particle sizes, revealing the relatively higher aromaticity and more freshness of WSOC in smaller particles. The carboxylic groups tend to be enriched in larger particles, whereas the contribution of phenolic groups was generally higher in smaller particles than that in larger particles. Overall, the chromophores in smaller particles showed a more pronounced pH dependence, revealing that the chromophores in smaller particles were more pH-sensitive. The change in the fluorescence peak position suggested that hydroxyl groups play a leading role in pH-responsive fluorescence in summer, while carboxylic groups in winter. WSOC with sizes of < 0.77 μm mainly originate from primary combustion emissions, and those with sizes of 1.40–2.50 μm primarily originate from secondary formations. Overall, the pH-dependent and particle size-dependent behaviors of aerosols WSOC provide insights into the structure, aging, and source of WSOC, and ultimately contribute to improving the accuracy of assessing the climate effects of WSOC.

https://doi.org/10.5194/acp-2022-321
Preprint. Discussion started: 18 May 2022

Atmospheric Chemistry and Physics Discussions

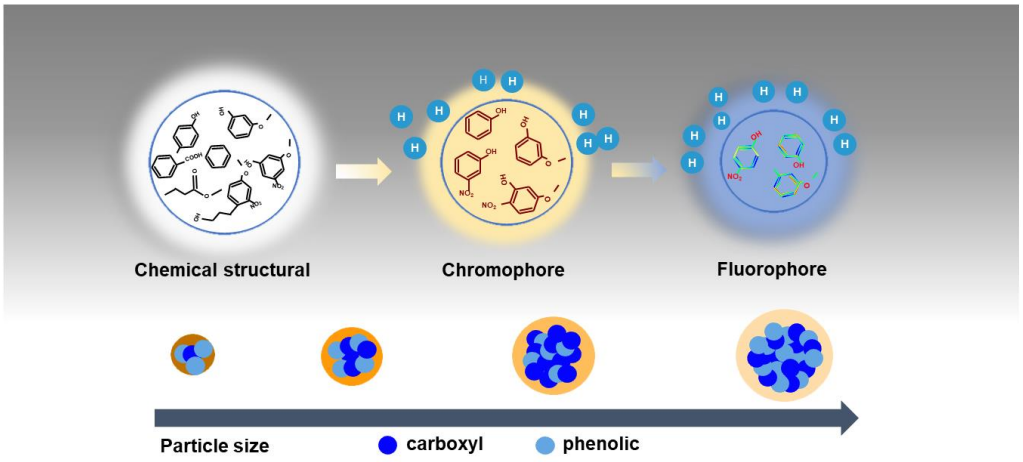

Graphical abstract

1 Introduction

Atmospheric particulate matter, derived from both primary emissions and secondary production, is a complex mixture with particle sizes ranging from 1 to 100 μm (Chalbot et al., 2021). They have a key role for many physicochemical processes in the atmosphere and other environmental systems (Horník et al., 2021). Atmospheric particulate matter are traditionally classified into two major classes: fine particles (particles with an aerodynamic diameter ≤ 2.5 μm) and coarse particles (particles with an aerodynamic diameter > 2.5 μm) (Boreddy et al., 2021). The physicochemical speciation of different particle sizes can serve as a good indicator of their sources, formation processes, and atmospheric aging (Xie et al., 2021).

Water-soluble organic carbon (WSOC) comprises a considerable fraction of organic aerosol mass (10 %–80 %) (Horník et al., 2021). Numerous studies have shown that WSOC are primarily derived from the biomass combustion and atmospheric oxidation reactions of organic compounds (Yu et al., 2017; Park et al., 2015; Du et al., 2014), with a relatively small contribution from fossil fuel burning emissions (Yu et al., 2017). Owing to its strong absorption of solar radiation and surface

https://doi.org/10.5194/acp-2022-321
Preprint. Discussion started: 18 May 2022


Atmospheric Chemistry and Physics Discussions

activity, WSOC plays a key role in climate change (Chen et al., 2020; Chen et al., 2016; Sun et al., 2011). Additionally, WSOC also has a negative impact on air quality and human health. The chemical composition of submicron particles (< 1 μm) has the most significant impact on cloud-forming efficiency and will enter the alveoli and bloodstream easier (Kroflič et al., 2018; Lin and Lee, 2004), thus, WSOC in submicron particles may have more serious effects on climate and human health than $PM_{2.5}$. It has been widely believed that aerosol WSOC properties are related to particle size (Chen et al., 2019). WSOC in different particle sizes can provide important information about their source, aging, fate, and haze pollution process (Ni et al., 2021; Jang et al., 2019; Chen et al., 2019). Hence, the variation characteristics, such as the optical and chemical properties, of WSOC of different particle sizes are required to further illustrate the physicochemical processes of aerosol WSOC. Previous studies have been performed to investigate the size distributions of WSOC and their particle size related optical properties (Chen et al., 2019; Liu et al., 2013). More recently, Qin et al. (2021a) investigated the fluorescence characteristics of size-resolved WSOC, and they found that the concentration and fluorescence properties of WSOC varied with the particle size, and the fluorescence characteristics of different particle sizes could be used to reveal the aging of WSOC. Despite the increasing awareness of the importance of particle size, there currently remains a knowledge gap regarding WSOC aging, fate and the size of their environmental impact in the atmosphere because the research on WSOC with different particle sizes is still limited.

Environmental conditions, such as relative humidity (RH), solar radiation intensity, and temperature, can affect the physical and chemical properties of aerosol particles (Bousiotis et al., 2021; Ge et al., 2021), especially aerosol acidity (pH). Aerosol pH affects the formation of secondary organic aerosols (SOA) via altering chemical reaction pathways (Ault, 2020), ultimately affecting the global climate. However, due to the complexity of the physicochemical properties of aerosols with particle sizes, our understanding of their pH is still limited, especially the pH-dependent behavior of such WSOCs, which have not been documented. Thus, examining the pH-dependent of WSOC with different particle sizes would be a worthy attempt to help identify their formation mechanisms and aging.

To better understand the structure, aging, and source of WSOC, this study explored the chemical structure and optical properties from the perspective of pH and particle size response. Firstly, the functional groups of four WSOC with representative particle sizes of < 0.26, 0.44–0.77, 1.40–2.50, and 2.50–10.0 μm were analyzed using a Fourier transform infrared spectroscopy (FTIR) and pH titration. Then, the optical properties of WSOC were determined with an ultraviolet–

https://doi.org/10.5194/acp-2022-321
Preprint. Discussion started: 18 May 2022


Atmospheric Chemistry and Physics Discussions

visible (UV–Vis) absorption spectroscopy and excitation-emission matrix (EEM) fluorescence spectroscopy combined with parallel factor analysis (PARAFAC). Subsequently, we examined the influence of pH on the optical properties of WSOC with different particle sizes. Finally, the environmental implications of pH-dependent and particle size-dependent behaviors of WSOC were discussed.

2 Experimental methods

2.1 Sample collection and preparation.

2.1.1 Sample collection

Particulate samples were collected on the roof of Teaching Building #1 (40°24′N, 116°40′E) of the University of Chinese Academy of Sciences (~20 m above the ground) in Huairou District of Beijing, China, during the months of June, 2019 to August, 2020. A total of 82 samples were collected on prebaked (under 550°C for 4.5 h) quartz fiber filters (Φ 90 mm, Whatman) using a 6-stage micro-orifice uniform deposit impactor (MOUDI), with aerodynamic cut-point diameters of 0.26, 0.44, 0.77, 1.40, 2.50, and 10.0 μm. All the samples were collected from 8 a.m. to 7 a.m. of the next day. The collected samples were then stored at −20°C until further analysis.

2.1.2 WSOC extraction

A quarter of all filters for each season were combined for WSOC extraction, similar to previous studies (Qin et al., 2018). WSOC was extracted twice via ultrasonication in Milli-Q water for 15 min to achieve the extensive release of solubilized WSOC, and then the extracted liquid was filtered through a 0.22 μm membrane filter to remove insoluble suspensions. Blank filters, used for background checks, were also extracted under the same conditions.

2.1.3 pH titration

HCI and NaOH were used to adjust the pH of the WSOC solutions. The pH of the WSOC for UV–Vis absorption and EEM fluorescence spectrometry was controlled in the range of 2–10 at 1 unit interval and recorded using a pH meter (Mettler Toledo, Swiss). The pH meter was calibrated before running any titration.

https://doi.org/10.5194/acp-2022-321
Preprint. Discussion started: 18 May 2022


Atmospheric Chemistry and Physics Discussions

The distribution of acidic groups was also obtained by pH titration as described in detail elsewhere (Wang and Waite, 2009). Briefly, prior to titration, the 50 ml WSOC solutions were first acidified to a pH below 3 by addition of HCl solution, and then the titration was performed until the pH was higher than 10 by stepwise addition of 0.1 M NaOH. Throughout the titration, the WSOC solution was bubbled with pure N_2 to remove air.

2.2 Instrumental analyses.

2.2.1 Total organic carbon (TOC) and FTIR analysis

The WSOC concentration was quantified by a TOC analyzer (Analytic Jena AG multi N/C3100, Germany). Prior to measurement, a drop of 2 mol L^{-1} HCI was added to the WSOC solution to remove the interference of inorganic carbon.

A Perkin Elmer FTIR (Frontier) spectrometer was employed to investigate the functional groups of WSOC. A fully dried mixture of the lyophilized WSOC and KBr was ground in an agate mortar and pressed into discs for FTIR analysis. FTIR spectra were recorded in the range of 4000–400 cm^{-1} with a 1 cm^{-1} interval at a spectral resolution of 4 cm^{-1}. Pure KBr was measured under the same conditions and its spectra was subtracted from the sample spectra for background correction.

2.2.2 UV–Vis absorption and EEM fluorescence spectra.

UV–Vis absorption and EEM fluorescence spectra of WSOC were recorded in a 1 cm path-length quartz cell using an UV–visible spectrophotometer (UV–2401PC, Shimadzu, Japan) and a fluorescence spectrophotometer (Agilent Cary Eclipse, America), respectively. The UV–Vis absorption spectra for all samples were measured over the wavelength range from 200 to 500 nm with an interval of 1 nm. The EEM fluorescence spectra were recorded in the wavelength range of 200 to 400 nm for excitation and 250 to 500 nm for emission with an interval of 5 nm.

2.3 Data analysis.

2.3.1 Acidic group distributions

The distribution of acidic groups (pK_a and group density), was calculated by the pH titration data using linear programming optimization as follows (Wang and Waite, 2009):

https://doi.org/10.5194/acp-2022-321
Preprint. Discussion started: 18 May 2022

Atmospheric Chemistry and Physics Discussions

$$\sum C_j\alpha_{ij} - C_{ANC} = [base] - [acid] - [carb] + [H^+] - [OH^-] , \quad (1)$$

$$\alpha_{ij} = \frac{K_{aj}}{K_{aj}+[H^+]} , \quad (2)$$

where the term $\Sigma C_j\alpha_{ij}$ is the sum of unreacted functional groups at each titration step (i = 1, m), C_j denotes the concentration of the j^{th} functional group, K_{aj} (j=1, n) represents the conditional dissociation constants ($K_{aj}=10^{-pKaj}$), and C_{ANC} denotes the acid-neutralizing capacity of the system (defined as the sum of all non-reacting cations minus non-reacting anions). The concentrations of acid ([acid]) and carbonate ([carb]=$[HCO_3^-]+2[CO_3^{2-}]$) were zero in this study since the titration starting pH was below 3.

2.3.2 UV–Vis absorption spectra

Based on the UV–Vis absorption spectra, the spectral slope at a wavelength of 275–295 nm ($S_{275-295}$), specific UV absorbance at wavelength of 254 nm ($SUVA_{254}$, $m^2\ g^{-1}$), mass absorption efficiency (MAE_λ, $m^2\ g^{-1}$), Absorption Ångström Exponent (AAE), and the difference absorbance spectra (Δabsorbance (λ), $m^2\ g^{-1}$) were calculated according to the following Eq. (Jane et al., 2017):

$$A_\lambda = A_{\lambda 0} e^{-S(\lambda-\lambda 0)} , \quad (3)$$

$$SUVA_{254} = \frac{A_{254}}{C\times L} , \quad (4)$$

$$MAE_\lambda = \frac{A_\lambda}{C\times L}\times \ln(10) , \quad (5)$$

$$MAE_\lambda = K\times\lambda^{-AAE}\ (330\ nm \le \lambda \le 400\ nm) , \quad (6)$$

$$\Delta absorbance\ (\lambda) = \frac{A(\lambda)_{pH} - A(\lambda)_{ref}}{C\times L} , \quad (7)$$

where A_λ denotes the absorbance at wavelength λ, λ_0 is the reference wavelength, C is the mass concentration of WSOC, L is the cell path length (1 cm), and K is a constant related to light absorption. Additionally, the $A(\lambda)_{pH}$ and $A(\lambda)_{ref}$ are the absorption spectra at a different pH and at a reference pH (2 and 7), respectively.

2.3.3 EEM and PARAFAC analysis

The raw EEM spectra were processed using the following procedure described in detail elsewhere (Xiao et al., 2018b). The

https://doi.org/10.5194/acp-2022-321
Preprint. Discussion started: 18 May 2022


Atmospheric Chemistry and Physics Discussions

pure water was subtracted from the EEM spectra of WSOC as background correction. The UV–Vis absorbance in the wavelength range of 200–500 nm was used to correct for the inner-filter effect of fluorescence intensity. Subsequently, the fluorescence intensity was normalized to Raman units (RU) using the Raman peak area of pure water, and was further divided by the TOC concentration to obtain the specific fluorescence intensity per unit TOC (SFI). Detailed information on EEM fluorescence properties such as fluorescence intensity per unit TOC of emission spectra (FI_m/TOC), apparent quantum yield (AQY), and Stokes shift were further extracted. AQY is defined as the ratio of the number of emitted photons to the number of absorbed photons after the fluorophores absorbing light (Xiao et al., 2018b). The Stokes shift, is defined as the difference between the excitation and emission wavenumbers, and they can be calculated as follows:

$$\mathrm{SFI}=\frac{\mathrm{FI}}{\mathrm{TOC}}=\frac{1}{\mathrm{TOC}}\left(\frac{1}{N}\sum_{\mathrm{Ex}}\sum_{\mathrm{Em}} I\right), \tag{8}$$

$$\frac{\mathrm{FI_m}}{\mathrm{TOC}}=\frac{1}{\mathrm{TOC}}\left(\frac{1}{N_{\mathrm{Ex}}}\sum_{\mathrm{Ex}} I\right), \tag{9}$$

$$\mathrm{AQY}=\frac{\int_{\mathrm{Em}}\mathrm{FI}(\lambda_{\mathrm{Ex}},\lambda_{\mathrm{Em}})\mathrm{d}\lambda_{\mathrm{Em}}}{\mathrm{UVA}(\lambda_{\mathrm{Ex}})\int_{\mathrm{Em}}\mathrm{d}\lambda_{\mathrm{Em}}}\Bigg|_{\mathrm{Ex}}, \tag{10}$$

$$\text{Stokes shift}=\frac{1}{\lambda_{\mathrm{Ex}}}-\frac{1}{\lambda_{\mathrm{Em}}}, \tag{11}$$

where FI is the fluorescence intensity, I is the fluorescence intensity at each Ex/Em wavelength position, N is the total number of EEM data, N_{Ex} denotes the total number of data under each Ex wavelength position, UVA is the average absorbance, and λ_{Ex} and λ_{Em} are the excitation and emission wavelengths (nm), respectively.

The different independent fluorescent components were identified by PARAFAC analysis using the DOM-Fluor toolbox (Wang et al., 2022). Three independent components were acquired in this study based on split half analysis, residual analysis, and visual inspection (Wu et al., 2011).

3 Results and discussion

3.1 Optical properties and chemical structures of WSOC

3.1.1 Optical properties at raw pH

The optical absorption and fluorescence properties of WSOC are presented in Table 1. Clearly, the optical absorption and

https://doi.org/10.5194/acp-2022-321
Preprint. Discussion started: 18 May 2022


Atmospheric Chemistry and Physics Discussions

fluorescence properties of WSOC with particle size were different. We found that the $S_{275–295}$ decreased with increasing particle size in summer. For winter WSOC, $S_{275–295}$ showed the highest value in 0.44–0.77 μm and the lowest value in 1.40–2.50 μm. These results indicate that the molecular weight of WSOC was higher for particle sizes of 2.50–10.0 μm in summer and 1.40–2.50 μm in winter (Helms et al., 2008; Shen et al., 2012). However, both summer and winter $SUVA_{254}$ were higher for particle sizes of < 0.26 μm than other particle sizes, highlighting the relatively higher aromaticity of WSOC in small particles (Cawley et al., 2013). This may be due to the more freshness of WSOC in the small particle size. For example, Fan et al. (2020) found that the aromaticity of chromophores in biomass burning decreased during the aging process. In contrast, larger particles were generally believed to be more aged than smaller particles because smaller particles would grow up to be larger particles via various the atmospheric aging process (Jang et al., 2019). The MAE_{365} values of < 0.26 μm, 0.44–0.77 μm, 1.40–2.50 μm, and 2.50–10.0 μm were 0.1258, 0.1321, 0.1014, and 0.1145 $m^2\ g^{-1}$ in summer and 1.2615, 0.7991, 0.8206, and 0.3707 $m^2\ g^{-1}$ in winter, indicating that WSOC of the smaller particles has a stronger light absorption capability (Wu et al., 2018). It should also be noted that MAE_{365} in winter was 3–10 times higher than that in summer, which can be inferred to be due to different sources and formation mechanisms of WSOC. It has been documented that more aromaticity and larger molecular sizes of light-absorbing substances tend to have higher MAE_{365}, which is mainly derived from biomass burning (Kim et al., 2016; Wu et al., 2018). However, MAE_{365} is lower for those with lower aromaticity or smaller molecular sizes from secondary formations due to the decomposition of aromatic compounds or photobleaching (Huang et al., 2018; Fan et al., 2020). This is also consistent with our previous study (Qin et al., 2022), where the MAE_{365} of combustion sources was significantly higher than that of ambient samples. Therefore, the seasonal difference in MAE_{365} further confirms that WSOC may be mainly derived from secondary formation in summer and from primary emissions (e.g., biomass burning, coal combustion, and vehicle exhaust) in winter.

Table 1. The optical properties of WSOC with different particle sizes (μm) at raw pH.

	< 0.26		0.44–0.77		1.40–2.50		2.50–10.0	
	Summer	Winter	Summer	Winter	Summer	Winter	Summer	Winter
$S_{275–295}$	0.0229	0.0151	0.0226	0.0160	0.0173	0.0148	0.0160	0.0157

https://doi.org/10.5194/acp-2022-321
Preprint. Discussion started: 18 May 2022


Atmospheric Chemistry and Physics Discussions

$SUVA_{254}$ ($m^2\ g^{-1}$)	0.0064	0.0317	0.0054	0.0237	0.0062	0.0181	0.0063	0.0093
MAE_{365} ($m^2\ g^{-1}$)	0.1258	1.2615	0.1321	0.7991	0.1014	0.8206	0.1145	0.3707
AAE	9.1573	5.4345	6.7218	6.3975	10.047	4.3854	5.2922	4.2987
FI/TOC (R.U. $mg^{-1}\ L^{-1}$)	0.0644	0.6973	0.0432	0.4440	0.0487	0.2408	0.0133	0.0990
AQY	0.2967	0.6261	0.2555	0.5993	0.2644	0.4242	0.0506	0.4826
Stokes shift (um^{-1})	0.0105	0.0173	0.0119	0.0190	0.0212	0.0154	0.0121	0.0128

The overall fluorescence properties including the average fluorescence intensity per TOC (FI/TOC), AQY, and Stokes shift are shown in Table 1. These fluorescence properties also differed among the different particle sizes of WSOC. The fluorescence intensity was higher for those fresh brown carbon (BrC) than for aged BrC, as previously observed by Fan et al. (2020). In this study, the overall FI/TOC decreased steadily with increasing particle size, which confirms that aged WSOC might have undergone a growth process with increasing particle size. AQY exhibited a similar trend to FI/TOC, indicating that a large scale of π-conjugated system and less electron-withdrawing groups (e.g. $–NH_3^+$ and –COOH) seem to be present in the smaller particle samples (Xiao et al., 2020; Xiao et al., 2018b). For summer WSOC, the Stokes shift of the particle size of 1.40–2.50 μm was higher than that of the other particle sizes, indicating greater energy loss due to relaxation in the excited states of the fluorophores in larger particles. For the winter, however, the particle sizes of 0.44–0.77 μm showed an even higher Stokes shift. It was interesting to note that there is a significant difference in the optical properties (e.g., $SUVA_{254}$, MAE_{365}, and FI/TOC) of WSOC for smaller particles in winter and summer, compared to a relatively slight difference in larger particles, suggesting that there are significant seasonal differences in the sources and chemical structures of WSOC in smaller particles.

3.1.2 Fourier transform infrared (FTIR) spectroscopy

The FTIR spectra can provide qualitative information about the different functional groups of WSOC in particles of different sizes, as presented in Fig. 1. The FTIR spectra predominantly exhibited the presence of oxygen containing functional groups and aliphatic C–H groups for both samples (Duarte et al., 2005). Strong absorptions of C−OH (3429 cm^{-1}) were observed for all samples, indicating that WSOC contained abundant phenol, hydroxyl, and carboxyl groups (Duarte et al., 2005). A weak absorption at 3175 cm^{-1} was observed in both < 0.26 μm and 0.44–0.77 μm samples, typically corresponding to the N–H

https://doi.org/10.5194/acp-2022-321
Preprint. Discussion started: 18 May 2022

Atmospheric Chemistry and Physics Discussions

stretching vibration of amide (Huo et al., 2008), but this feature was not shown in the spectra of the large particles, indicating a higher amide content in smaller particle sizes. In addition, an absorption peak at 1720 cm^{-1} was only present in the smallest particle sizes of < 0.26 μm in summer, which was attributed to the unconjugated C=O stretching mainly of carbonyl carbon (Hu et al., 2019). The peak at 1641 cm^{-1} was attributed to conjugated carbonyl (C=O) groups and aromatic rings (C=C), were also observed. A strong and sharp absorption at 1389 cm^{-1}, is usually attributed to the C–H asymmetric bending vibrations of methyl groups in aliphatic chains (Duarte et al., 2007; Colthup, 2012). These results suggest that WSOC of different sizes contain abundant branched structures. The presence of a peak at 1114 cm^{-1} typically corresponded to the stretching vibration of C–OH, mainly alcohol (Chen et al., 2017). Strong absorptions of the out-of-plane vibrations of C–H (625 cm^{-1}) and C=C (827 cm^{-1}) groups were observed in the spectra, indicating that WSOC also contained abundant alkenes (Duarte et al., 2007).

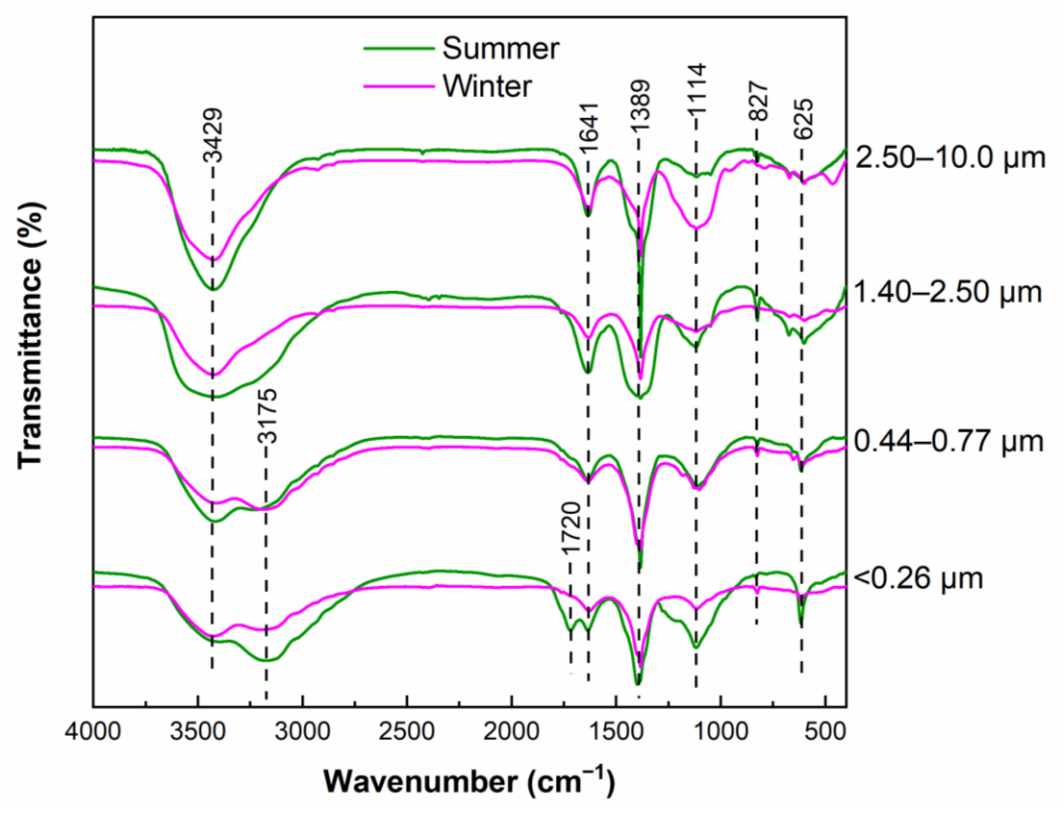

Figure 1. FTIR spectra of WSOC in particles of different sizes.

https://doi.org/10.5194/acp-2022-321
Preprint. Discussion started: 18 May 2022


Atmospheric Chemistry and Physics Discussions

3.1.3 Acidic group distribution

pH titration enables qualitative and quantitative analyses of functional groups on the surface of substances (Zhang et al., 2011; Xiao et al., 2014). However, measurements of such type have not yet been performed for particles with different sizes. Figure 2 shows the distributions of the acidic groups of WSOC with a pK_a range of 3.0–9.0. The pK_a values of carboxylic and phenolic groups are in the range of 3.5–5.6 and 8.1–9.0, respectively. The pK_a range of 6.3–7.9 may be an overlapping region among weak carboxylic groups, phosphoric acids or phenols (Mu et al., 2019).

The contribution of (strong) carboxylic groups showed a clear characteristic of particle size distribution, with the highest percentage in sizes of 1.40–2.50 μm and the lowest percentage in sizes of < 0.77 μm, reflecting that (strong) carboxylic groups tend to exist in larger particles, consistent with the above findings in AQY. In contrast, the contribution of (strong) phenolic groups was highest in smaller particles (< 0.77 μm) and lowest in larger particles (1.40–2.50 μm). This pattern indicates that the phenolic groups were abundant in smaller particle WSOC. It has been demonstrated that carboxylic acids are primarily associated with SOA sources (Glasius et al., 2022; Wang et al., 2021), while phenol is abundant in biomass combustion particles (Laskin et al., 2015; Lin et al., 2016). Thus, it can be concluded that WSOC with sizes of < 0.77 μm mainly originated from primary combustion emissions, and those with sizes of 1.40–2.50 μm primarily originated from secondary formations. Jang et al. (2019) also mentioned that smaller particles are likely derived from primary sources and larger particles are likely derived from secondary formation. Overall, compared to winter, the contribution of carboxyl was higher and the phenolic group was lower in summer. This result indicates that summer WSOC was mainly related to secondary generation, while winter WSOC was mainly derived from primary sources.

https://doi.org/10.5194/acp-2022-321
Preprint. Discussion started: 18 May 2022

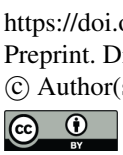

Atmospheric Chemistry and Physics Discussions

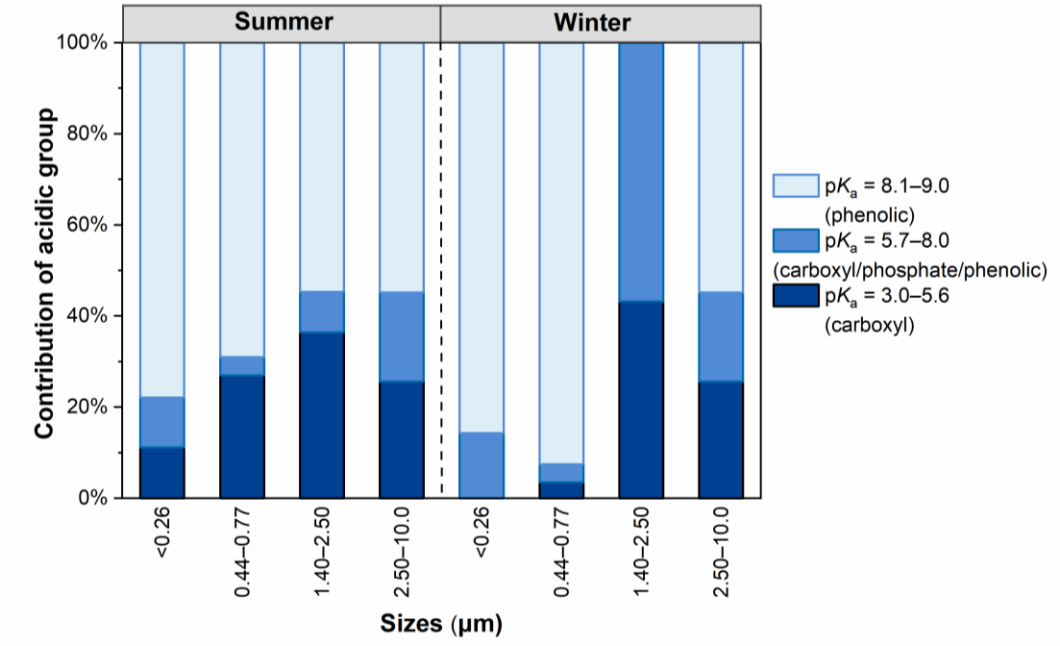

Figure 2. The distribution of the acidic group of WSOC in particles of different sizes.

3.2 Role of pH on UV–Vis absorption spectra

3.2.1 Absorption spectra

In addition to the particle size, the aerosol pH is another factor that must be considered, which affects the structure of WSOC chromophores. As shown in Fig. 3, a monotonic increase in the absorption of WSOC was observed with increasing pH for almost all samples, which may be related to the deprotonation of aromatic WSOC chromophores (Korshin et al., 1997; Young et al., 2018). On average, the absorbance for particle sizes of < 0.26 μm, 0.44–0.77 μm, 1.40–2.50 μm, and 2.50–10.0 μm increased by 4.57 %, 1.34 %, 0.63 %, and 0.93 % per unit pH increase in summer, respectively, and 1.34 %, 0.51 %, 0.48 %, and 2.88 % in winter, respectively. The results suggest that the chromophores in particle sizes of < 0.26 μm and 0.44–0.77 μm in summer and < 0.26 μm and 2.50–10.0 μm in winter showed a more pronounced pH dependence.

https://doi.org/10.5194/acp-2022-321
Preprint. Discussion started: 18 May 2022

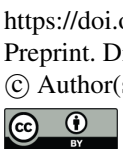

Atmospheric Chemistry and Physics Discussions

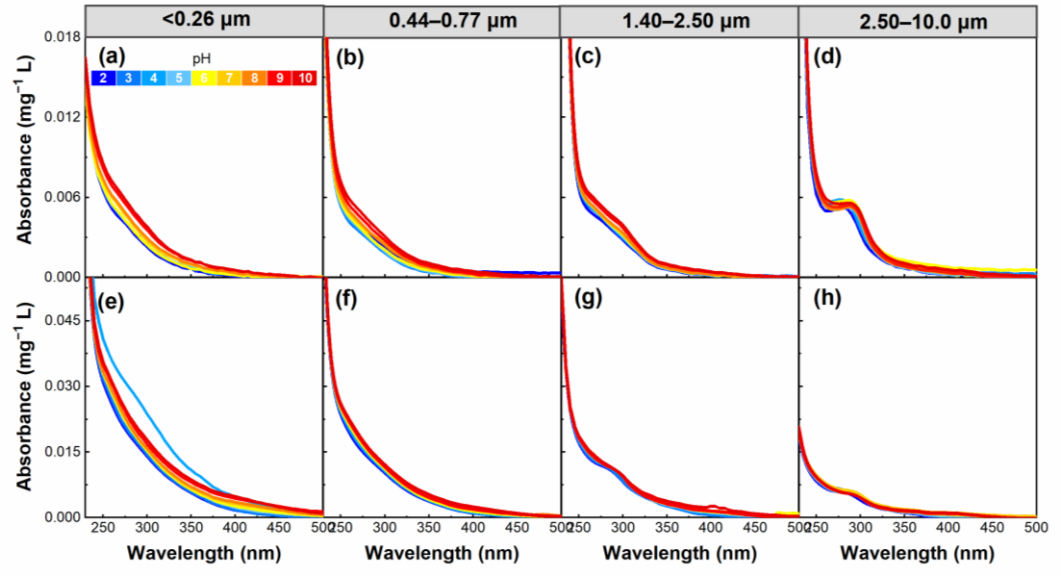

Figure 3. pH dependence of absorption per unit mass for WSOC in summer (a–d, a, < 0.26 μm; b, 0.44–0.77 μm; c, 1.40–2.50 μm; and d, 2.50–10.0 μm) and winter (e–h, e, < 0.26 μm; b, 0.44–0.77 μm; c, 1.40–2.50 μm; and d, 2.50–10.0 μm).

3.2.2 Difference absorbance spectra (Δabsorbance)

Following the work of Dryer et al. (2008), the difference absorbance spectra (Δabsorbance (λ)) were calculated in this study to examine the behavior of groups in resonance with chromophores in WSOC under pH titration, since Δabsorbance can identify whether specific spectral bands defined as carboxyl and phenolic groups that undergoes significant changes within their corresponding pH ranges. Based on the distribution of the pK_a values of carboxyl (3.0–5.6) and phenolic groups (>8.0), carboxyl plays a major role in the absorbance in the range of approximately pH 3.0–6.0, while phenolic groups should predominate at pH>8.0.

The results summarized in Fig. 4 show that the most notable feature bands of Δabsorbance at ~270 nm were observed for almost all samples in the pH 3.0–6.0 range associated with the carboxyl group (Phillips et al., 2017), although an absorption band at ~300 nm was also observed for particle sizes of >2.50 μm in summer and winter, suggesting the presence of at least two distinct chromophores deprotonated for particle sizes of >2.50 μm in this pH range (Liu et al., 2020). However, the

https://doi.org/10.5194/acp-2022-321
Preprint. Discussion started: 18 May 2022

Atmospheric Chemistry and Physics Discussions

absorption band at ~270 nm was not observed for particle sizes of 2.50–10.0 μm in summer, suggesting that the carboxyl deprotonation feature was inhibited compared to other samples. For the pH 8.0–10 range, an enhanced absorption band primarily centered between 300 and 400 nm, and this band is approximately the position of the phenolic group, indicating that phenolic groups play a major role in this pH range (Schendorf et al., 2019).

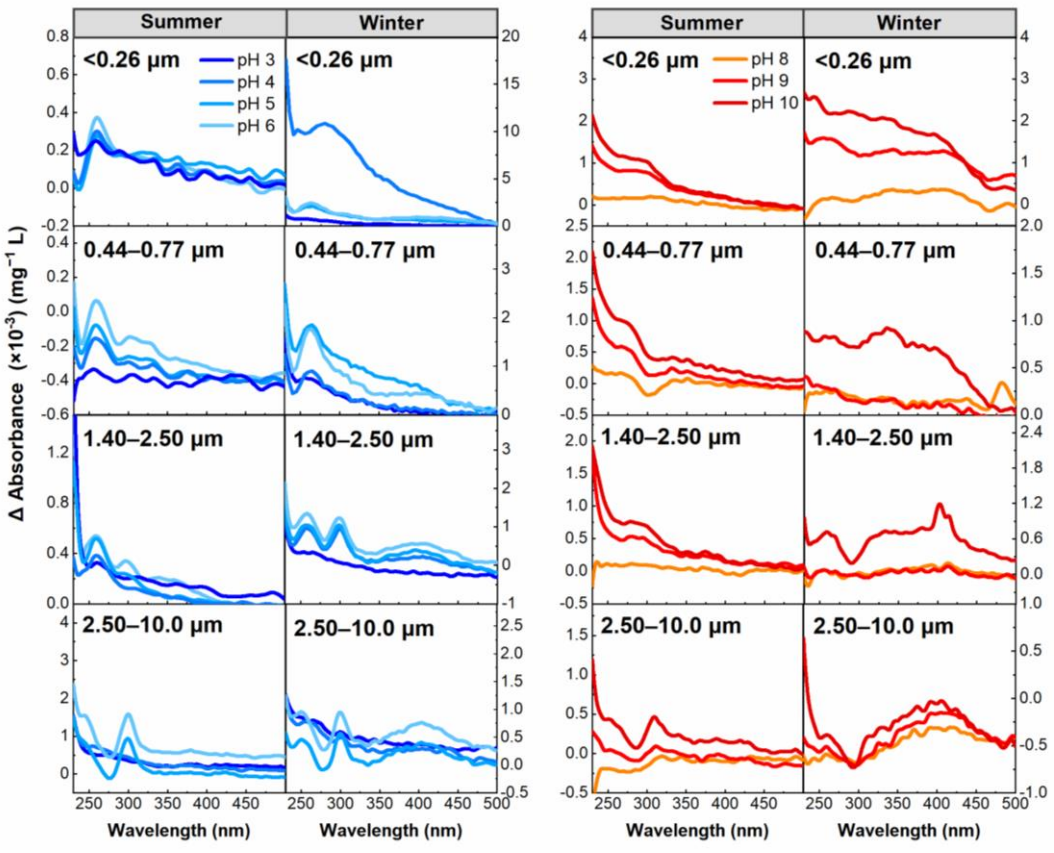

Figure 4. Difference absorbance spectra (Δabsorbance) of WSOC.

3.2.3 Mass absorption efficiency at 365 nm (MAE_{365})

Mass absorption efficiency is a key parameter for assessing the direct radiative forcing of light-absorbing substances (Zhang et al., 2021). As reported previously for other WSOC (Mo et al., 2017), the MAE_{365} values appeared to show a visible trend, that is, an overall increase in MAE_{365} was observed with increasing pH (Fig. 5). This indicates that WSOC had a stronger light

https://doi.org/10.5194/acp-2022-321
Preprint. Discussion started: 18 May 2022

Atmospheric Chemistry and Physics Discussions

absorption capability at high pH. Namely, WSOC with different pH has different effects on climate change, and WSOC would enhance their influence on climate change in an alkaline environment (Aiona et al., 2018). However, the MAE_{365} for particle sizes of < 0.26 μm in winter, exhibited higher values at pH 4, most likely because the particle sizes of < 0.26 μm were significantly influenced by the group of pK_a values near 4. Overall, the average MAE_{365} for particle sizes of < 0.26 μm changed more sharply in both summer (47.4 % relative to the mean level) and winter (39.9 % relative to the mean level).

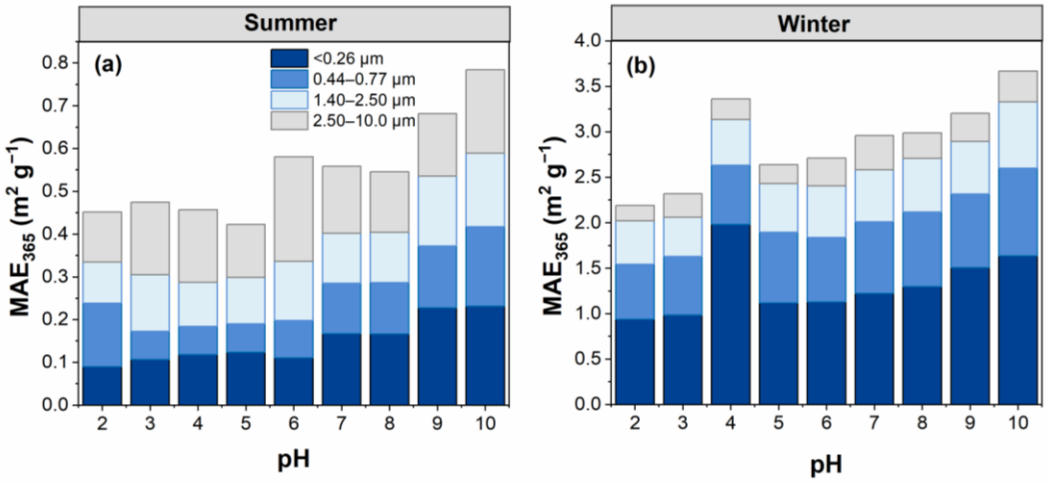

Figure 5. pH dependence of mass absorption efficiency (MAE_{365}) for WSOC in (a) summer and (b) winter.

3.3 Role of pH on EEM fluorescence spectra

3.3.1 EEM fluorescence properties

To examine the role of pH on the fluorescence intensity and peak position of WSOC from different particle sizes, the FI_m/TOC of WSOC was calculated from the EEM spectra and is plotted in Fig. 6. Overall, the FI_m/TOC of all samples generally decreased with increasing pH. This trend was verified by the results in Fig. 7, where from pH 2 to 10, the FI/TOC first slightly increased and then significantly decreased with increasing pH. On average, the FI/TOC of < 0.26 μm, 0.44–0.77 μm, 1.40–2.50 μm, and 2.50–10.0 μm decreased by 3.79 %, 3.47 %, 4.73 %, and 6.77 % per unit pH increase in winter, respectively, significantly more than the 0.58 %, 1.66 %, 0.18 %, 2.46 % in summer, respectively.

The different seasonal samples exhibited two different pH-dependent fluorescence behaviors. A redshift of fluorescence

https://doi.org/10.5194/acp-2022-321
Preprint. Discussion started: 18 May 2022

Atmospheric Chemistry and Physics Discussions

peak positions with increasing pH can be observed in summer (Fig. 7), but the opposite trend was observed in winter (blueshift) with increasing pH. Protonation and dissociation of the aromatic groups can generally lead to a shift in fluorophores (Coble et al., 2014; Schulman et al., 1985). For example, the dissociation of the electron withdrawing groups (e.g., carboxylic) leads to a blueshift in fluorophores, while the protonation of the electron donating groups (e.g., hydroxyl) results in a redshift in fluorophores (Schulman et al., 1985). In this regard, we speculate that the hydroxyl groups play a leading role in pH-responsive fluorescence in summer, while carboxylic groups play a dominant role in winter samples.

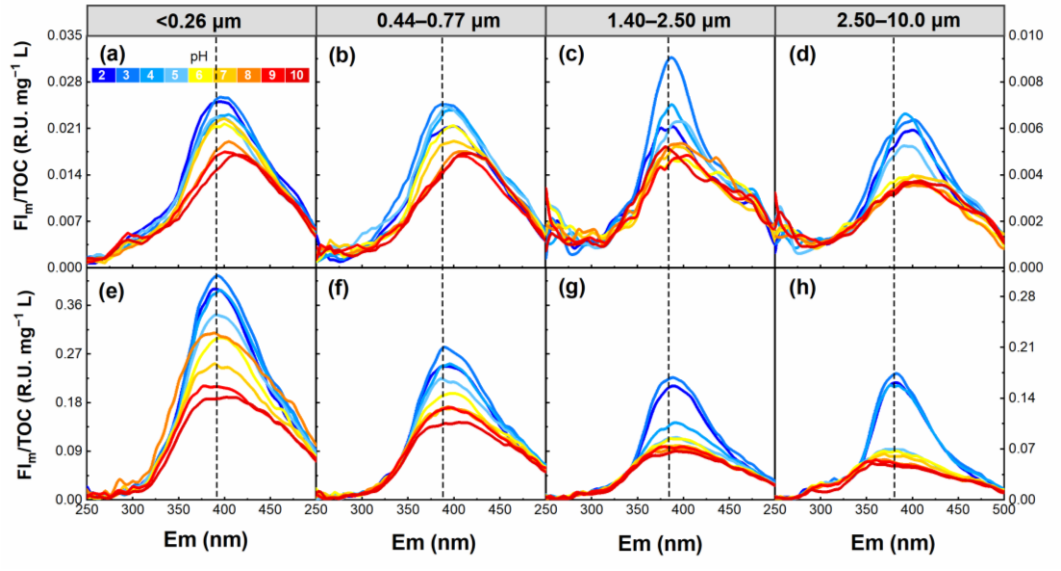

Figure 6. pH dependence of the FI_m/TOC for WSOC in summer (a–d) and winter (e–h).

https://doi.org/10.5194/acp-2022-321
Preprint. Discussion started: 18 May 2022

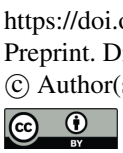

Atmospheric Chemistry and Physics Discussions

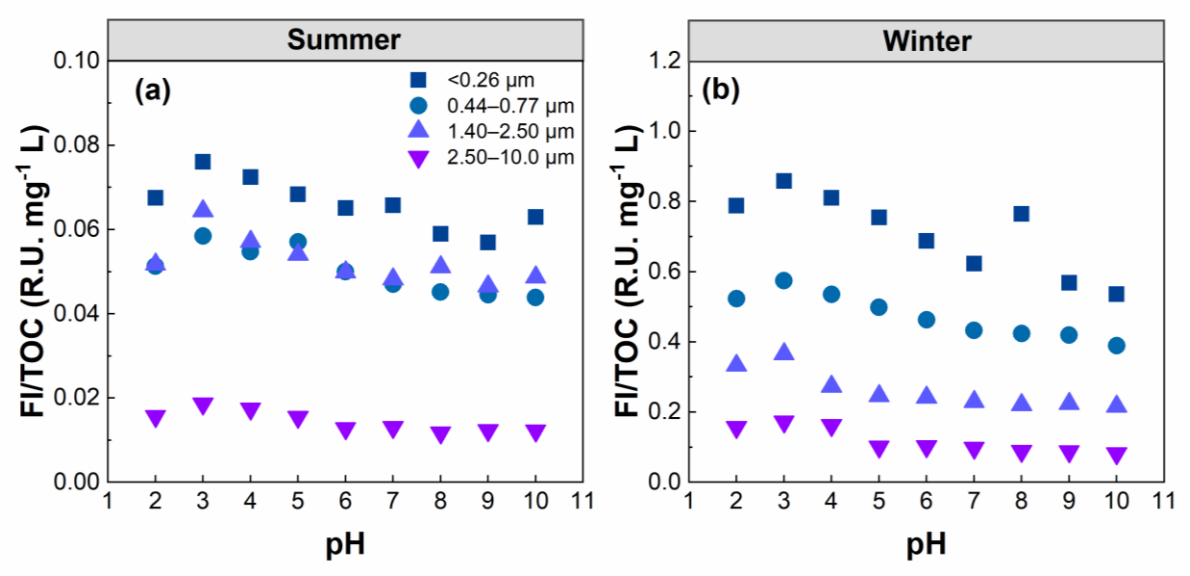

Figure 7. pH dependence of the FI/TOC for WSOC in summer (a) and winter (b).

3.3.2 PARAFAC Components

To investigate the types of fluorescence components in WSOC from different particle sizes, the EEM spectra were decomposed into three fluorescent components (C1, C2, and C3), as shown in Fig. 8. The chemical components corresponding to C1 and C2 were assigned to higher oxygenated humic-like (HULIS1) and less oxygenated humic-like (HULIS2) fluorophores, respectively (Qin et al., 2018; Qin et al., 2021b; Chen et al., 2016; Xiao et al., 2018a). C3 corresponds to protein-like organic matter (Chen et al., 2016).

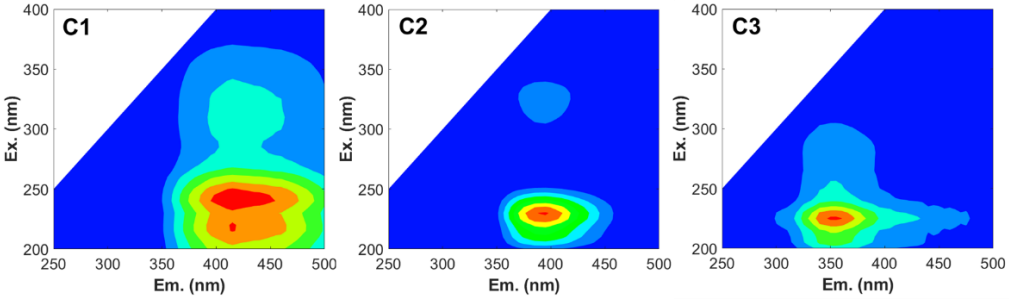

Figure 8. The fluorescence components (C1, C2, and C3) were identified using PARAFAC analysis for all WSOC samples.

https://doi.org/10.5194/acp-2022-321
Preprint. Discussion started: 18 May 2022

Atmospheric Chemistry and Physics Discussions

The peak intensities of the fluorescent components (F_{max}) are shown in Fig. 9. The F_{max} of the fluorescence components of WSOC at different pH were also different. The F_{max} of the fluorescence components showed a peak at pH 3, and then tended to decrease with increasing pH. In particular, the HULIS2 substances decreased sharply in the order of 0–0.26 μm >2.50–10.0 μm > 1.40–2.50 μm > 0.44–0.77 μm in summer, and 0–0.26 μm > 2.50–10.0 μm > 0.44–0.77 μm > 1.40–2.50 μm in winter. However, the variation in HULIS1 and protein-like organic matter was not obvious. Thus, the HULIS2 fluorophores showed the most susceptibility to acidity, especially in particle sizes of < 0.26 μm and 2.50–10.0 μm, suggesting that the specific fluorophore of WSOC was veries sensitive to pH due to structural differences.

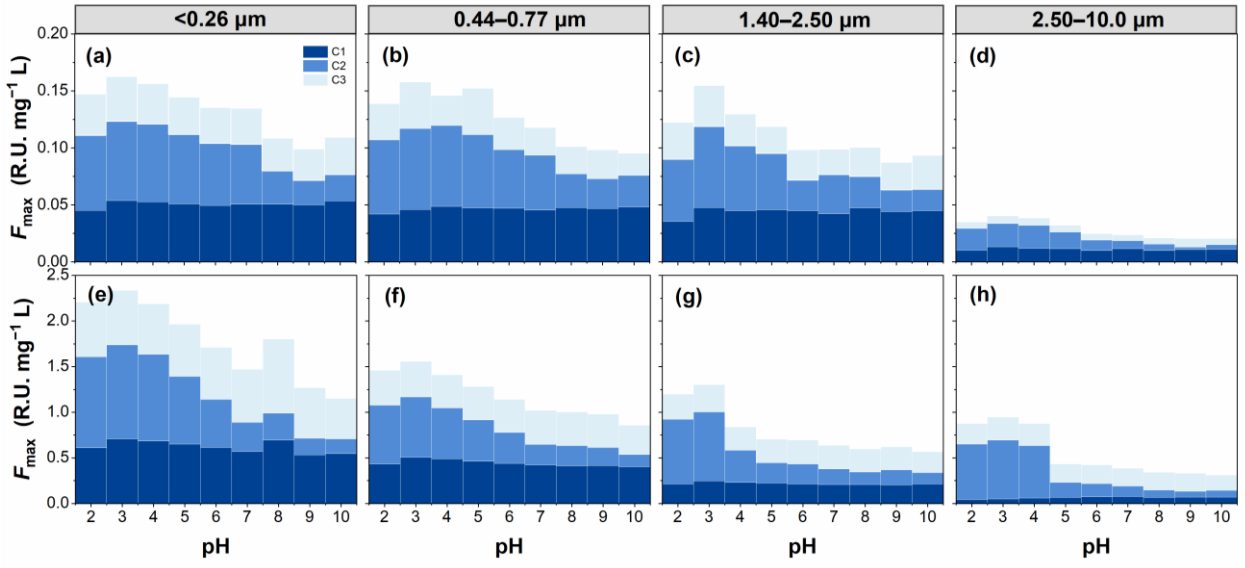

Figure 9. pH dependence of the F_{max} of fluorescence components for WSOC in summer (a–d) and winter (e–h).

3.3.3 Deep properties of fluorescence

AQY is an important parameter for understanding the effect of materials on climate. The high efficiency of WSOC fluorescence means that only a small portion of the absorbed radiative energy is converted into heat, thus reducing the heating effect of WSOC (Aiona et al., 2018). The change in AQY over the pH 2–10 range is plotted in Fig. 10. In all of WSOC samples, AQY was also presented as pH-dependent. AQY generally decreased with increasing pH, which was in agreement with our

https://doi.org/10.5194/acp-2022-321
Preprint. Discussion started: 18 May 2022

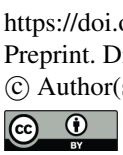

Atmospheric Chemistry and Physics Discussions

previous conclusion (Qin et al., 2021b). Hence, alkaline conditions would enhance the impact of WSOC on climate. Additionally, a larger rate of non-radiative transition seems to be favorable for the AQY of fluorophores (Xiao et al., 2020). This indicates that pH had an important effect on the rate of non-radiative transition of the fluorophores.

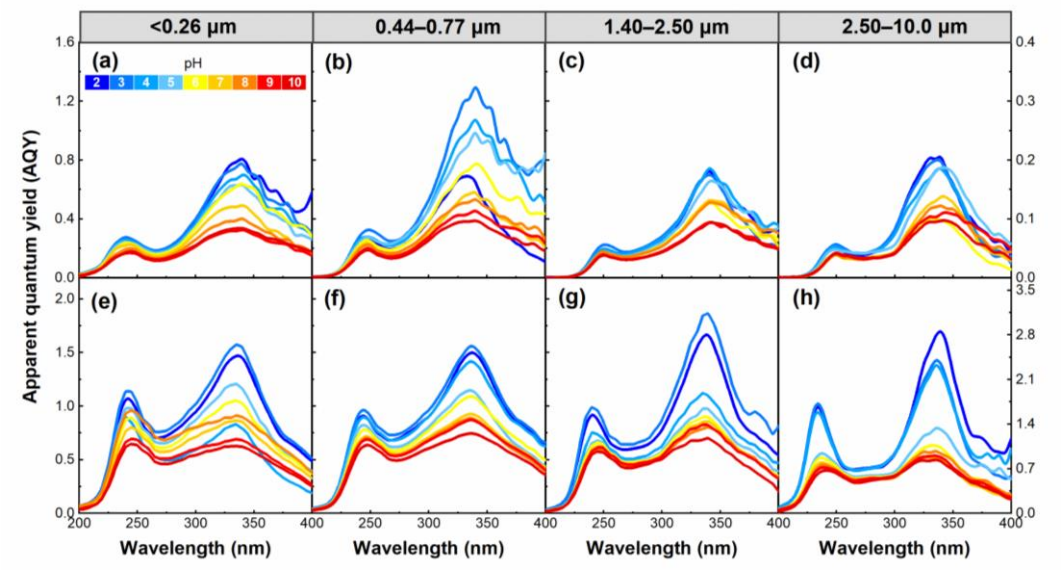

Figure 10. pH dependence of apparent quantum yield (AQY) for WSOC in summer (a–d) and winter (e–h).

The Stokes shift is an important energy parameter of fluorescence that can be affected by the chemical environment of the fluorophore (Xiao et al., 2019). As shown in Fig. 11, there was a common feature in all samples that WSOC had two distinct peaks at Stokes shifts around 0.7 and 2.0 μm. However, lower pH had stronger peaks at larger Stokes shift values (about 2.0 μm^{-1}), and this trend was clearly evident in winter samples, further suggesting that pH had an important impact on the π-conjugated systems of WSOC. Furthermore, summer WSOC tend to have higher Stokes shifts (at about 2.0 μm^{-1}) at higher pH, except for samples with a particle size of 2.50-10.0 μm. In contrast, winter samples usually have lower Stokes shifts (at about 2.0 μm^{-1}) at higher pH.

https://doi.org/10.5194/acp-2022-321
Preprint. Discussion started: 18 May 2022

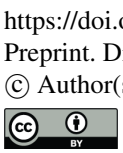

Atmospheric Chemistry and Physics Discussions

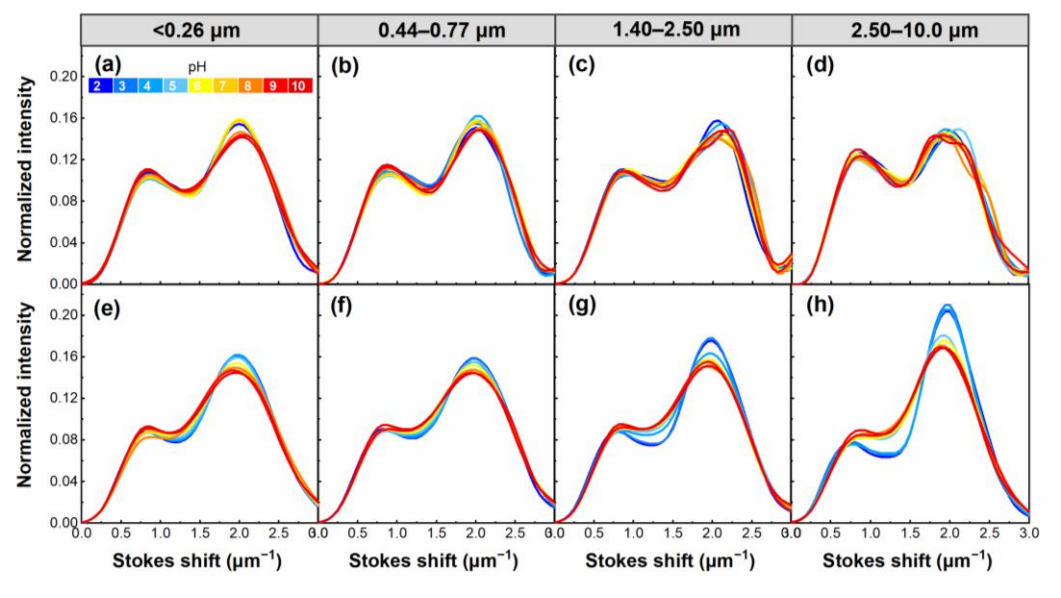

Figure 11. pH dependence of the Stokes shift for WSOC in summer (a–d) and winter (e–h).

4 Summaries and practical implications

In this study, we examined how the chemical structures and optical properties of WSOC were affected by pH and particle size, which may vary depending on season, source, and particle aging. For different particle sizes, higher $SUVA_{254}$, MAE_{365}, and FI/TOC were observed in smaller particle sizes, suggesting the relatively higher aromaticity and more freshness of WSOC in smaller particles. The distributions of acidic groups of WSOC indicated that the carboxylic groups tend to enrich in larger particles, whereas the contribution of phenolic groups was highest in smaller particles (< 0.77 μm) and lowest in larger particles (1.40–2.50 μm). These results demonstrated that WSOC with sizes of < 0.77 μm mainly originated from primary combustion emissions, and those with sizes of 1.40–2.50 μm primarily originated from secondary formations. Compared to large particles, the most significant seasonal differences in the optical properties (e.g., $SUVA_{254}$, MAE_{365}, and FI/TOC) were observed for WSOC with small particle sizes, suggesting that there are significant seasonal differences in the sources and chemical structures of WSOC in smaller particles. For different pH responsive properties, MAE_{365} generally increased with increasing pH, indicating WSOC had a stronger light absorption capability at high pH, in which smaller particles showed much higher susceptibility to pH change. However, FI/TOC, F_{max}, and AQY showed a peak at pH 3, and then significantly decreased with

https://doi.org/10.5194/acp-2022-321
Preprint. Discussion started: 18 May 2022


Atmospheric Chemistry and Physics Discussions

345 increasing pH. Among them, the HULIS2 fluorophores showed the most susceptibility to acidity.

These results suggest that the chemical characteristics and optical properties of WSOC with different particle sizes can provide an indication of information on their sources and atmospheric aging processes. The light absorption of WSOC increased with increasing pH, suggesting that the ability of such WSOC to influence climate was enhanced at high pH (Phillips et al., 2017; Aiona et al., 2018). However, aerosol pH is often acidic and acidity decreases with increasing particle size 350 (Battaglia et al., 2017; Craig et al., 2018). In this regard, the radiative forcing of WSOC in real atmospheric environments may be overestimated if the effect of pH is not considered, especially for WSOC in smaller particulate matter. For example, aerosol radiative forcing may be overestimated based on aerosol pH values at 7 instead of those at lower values, such as pH 2 (Pandey et al., 2020). In contrast to larger particle size samples, pH had a more significant effect on the light absorption properties of the smaller particle size samples, which may represent a significant effect of pH on fresh WSOC compared to aged WSOC, 355 consistent with our previous study finding a more significant effect of pH on the light absorption properties of fresh WSOC emitted from combustion sources (Qin et al., 2022). These findings are of great important implications for applying optical properties for chemical structure identification and source apportionment of WSOC and improving the accuracy of assessing the climate effects of WSOC. pH is also involved in aerosol multiphase chemical processes (e.g., gas-aerosol phase partitioning) (Craig et al., 2018). To better understand the mechanisms of many key atmospheric processes of WSOC, the reaction processes 360 of WSOC under real atmospheric conditions, should be comprehensively studied in the future.

Data availability. The data used in this study are given in the Supplement.

Author contribution. JT and YZ designed the experiments and finalized the article. YQ, JQ, and YG performed the measurements. YQ performed the data analysis and wrote the article with the assistance of KX. XW collected the samples. TQ, 365 XZ, SS, and JL provided useful comments on the article. JG, ZZ, and RC discussed the results.

Disclaimer. Publisher's note: Copernicus Publications remains neutral with regard to jurisdictional claims in published maps and institutional affiliations.

Competing interests. The authors declare that they have no conflict of interest.

https://doi.org/10.5194/acp-2022-321
Preprint. Discussion started: 18 May 2022

Atmospheric Chemistry and Physics Discussions

Acknowledgments. This work was supported by the National Natural Science Foundation of China (41675127 and 41975168).

References

Aiona, P. K., Luek, J. L., Timko, S. A., Powers, L. C., Gonsior, M., and Nizkorodov, S. A.: Effect of photolysis on absorption and fluorescence spectra of light-absorbing secondary organic aerosols, ACS. Earth. Space. Chem., 2, 235–245, http://dx.doi.org/10.1021/acsearthspacechem.7b00153, 2018.

Ault, A. P.: Aerosol acidity: Novel measurements and implications for atmospheric chemistry, Acc. Chem. Res., 53, 1703–1714, http://dx.doi.org/10.1021/acs.accounts.0c00303, 2020.

Battaglia, M. A., Douglas, S., and Hennigan, C. J.: Effect of the Urban Heat Island on Aerosol pH, Environ. Sci. Technol., 51, 13095–13103, http://dx.doi.org/10.1021/acs.est.7b02786, 2017.

Boreddy, S. K. R., Hegde, P., and Aswini, A. R.: Chemical characteristics, size distributions, and aerosol liquid water in size-resolved coastal urban aerosols allied with distinct air masses over tropical peninsular India, ACS. Earth. Space. Chem., 5, 457–473, http://dx.doi.org/10.1021/acsearthspacechem.0c00282, 2021.

Bousiotis, D., Brean, J., Pope, F. D., Dall'Osto, M., Querol, X., Alastuey, A., Perez, N., Petäjä, T., Massling, A., and Nøjgaard, J. K.: The effect of meteorological conditions and atmospheric composition in the occurrence and development of new particle formation (NPF) events in Europe, Atmos. Chem. Phys., 21, 3345–3370, http://dx.doi.org/10.5194/acp-21-3345-2021, 2021.

Cawley, K. M., McKnight, D. M., Miller, P., Cory, R., Fimmen, R. L., Guerard, J., Dieser, M., Jaros, C., Chin, Y.-P., and Foreman, C.: Characterization of fulvic acid fractions of dissolved organic matter during ice-out in a hyper-eutrophic, coastal pond in Antarctica, Environ. Res. Lett., 8, 045–015, http://dx.doi.org/10.1088/1748-9326/8/4/045015, 2013.

Chalbot, M. C., Siddiqui, S., and Kavouras, I. G.: Molecular speciation of size fractionated particulate water-soluble organic carbon by two-dimensional nuclear magnetic resonance (NMR) spectroscopy, Int. J. Environ., 18, 1334, http://dx.doi.org/10.3390/ijerph18031334, 2021.

Chen, Q., Ikemori, F., Nakamura, Y., Vodicka, P., Kawamura, K., and Mochida, M.: Structural and light-absorption characteristics of complex water-insoluble organic mixtures in urban submicrometer aerosols, Environ. Sci. Technol., 51, 8293–8303, http://dx.doi.org/10.1021/acs.est.7b01630, 2017.

Chen, Q., Mu, Z., Song, W., Wang, Y., Yang, Z., Zhang, L., and Zhang, Y. L.: Size-resolved characterization of the chromophores in atmospheric particulate matter from a typical coal-burning city in China, J. Geophys. Res. Atmos., 124, 10546–10563, http://dx.doi.org/10.1029/2019JD031149, 2019.

Chen, Q., Li, J., Hua, X., Jiang, X., Mu, Z., Wang, M., Wang, J., Shan, M., Yang, X., and Fan, X.: Identification of species and sources of atmospheric chromophores by fluorescence excitation-emission matrix with parallel factor analysis, Sci. Total. Environ., 718, 137322, http://dx.doi.org/10.1016/j.scitotenv.2020.137322, 2020.

Chen, Q., Miyazaki, Y., Kawamura, K., Matsumoto, K., Coburn, S., Volkamer, R., Iwamoto, Y., Kagami, S., Deng, Y., Ogawa, S., Ramasamy, S., Kato, S., Ida, A., Kajii, Y., and Mochida, M.: Characterization of chromophoric water-soluble organic matter in urban, forest, and marine aerosols by HR-ToF-AMS analysis and excitation–emission matrix spectroscopy, Environ. Sci. Technol., 50, 10351–10360, http://dx.doi.org/10.1021/acs.est.6b01643, 2016.

Coble, P., Lead, J., Baker, A., Reynolds, D. M., and Spencer, R.: Aquatic Organic Matter Fluorescence, Cambridge University Press, New York, USA, 2014.

Colthup, N.: Introduction to infrared and Raman spectroscopy, Academic press, New York and London, 2012.

Craig, R. L., Peterson, P. K., Nandy, L., Lei, Z., Hossain, M. A., Camarena, S., Dodson, R. A., Cook, R. D., Dutcher, C. S., and Ault, A. P.: Direct determination of aerosol pH: size-resolved measurements of submicrometer and supermicrometer aqueous particles, Anal. Chem., 90, 11232–11239, http://dx.doi.org/10.1021/acs.analchem.8b00586, 2018.

Dryer, D. J., Korshin, G. V., and Fabbricino, M.: In situ examination of the protonation behavior of fulvic acids using differential absorbance spectroscopy, Environ. Sci. Technol., 42, 6644–6649, http://dx.doi.org/10.1021/es800741u, 2008.

Du, Z., He, K., Cheng, Y., Duan, F., Ma, Y., Liu, J., Zhang, X., Zheng, M., and Weber, R.: A yearlong study of water-soluble organic carbon in Beijing I: Sources and its primary vs. secondary nature, Atmos. Environ., 92, 514-521, http://dx.doi.org/10.1016/j.atmosenv.2014.04.060, 2014.

Duarte, R. M. B. O., Pio, C. A., and Duarte, A. C.: Spectroscopic study of the water-soluble organic matter isolated from atmospheric aerosols collected under different atmospheric conditions, Anal. Chim. Acta, 530, 7–14, http://dx.doi.org/10.1016/j.aca.2004.08.049, 2005.

Duarte, R. M. B. O., Santos, E. B. H., Pio, C. A., and Duarte, A. C.: Comparison of structural features of water-soluble organic matter from atmospheric aerosols with those of aquatic humic substances, Atmos. Environ., 41, 8100–8113, http://dx.doi.org/10.1016/j.atmosenv.2007.06.034, 2007.

Fan, X., Cao, T., Yu, X., Wang, Y., Xiao, X., Li, F., Xie, Y., Ji, W., Song, J., and Peng, P. a.: The evolutionary behavior of chromophoric brown carbon during ozone aging of fine particles from biomass burning, Atmos. Chem. Phys., 20, 4593–4605, http://dx.doi.org/10.5194/acp-20-4593-2020, 2020.

Ge, M., Tong, S., Wang, W., Zhang, W., Chen, M., Peng, C., Li, J., Zhou, L., Chen, Y., and Liu, M.: Important oxidants and their impact on the environmental effects of aerosols, J. Phys. Chem. A., 125, 3813–3825, http://dx.doi.org/10.1021/acs.jpca.0c10236, 2021.

Glasius, M., Thomsen, D., Wang, K., Iversen, L. S., Duan, J., and Huang, R. J.: Chemical characteristics and sources of organosulfates, organosulfonates, and carboxylic acids in aerosols in urban Xi'an, Northwest China, Sci. Total. Environ., 810, 151187, http://dx.doi.org/10.1016/j.scitotenv.2021.151187, 2022.

Helms, J. R., Stubbins, A., Ritchie, J. D., Minor, E. C., Kieber, D. J., and Mopper, K.: Absorption spectral slopes and slope ratios as indicators of molecular weight, source, and photobleaching of chromophoric dissolved organic matter, Limnol. Oceanogr., 53, 955–969, http://dx.doi.org/10.4319/lo.2008.53.3.0955, 2008.

Horník, Š., Sýkora, J., Pokorná, P., Vodička, P., Schwarz, J., and Ždímal, V.: Detailed NMR analysis of water-soluble organic compounds in size-resolved particulate matter seasonally collected at a suburban site in Prague, Atmos. Environ., 267, 118757, http://dx.doi.org/10.1016/j.atmosenv.2021.118757, 2021.

Hu, B., Wang, P., Wang, C., Qian, J., Bao, T., and Shi, Y.: Investigating spectroscopic and copper-binding characteristics of organic matter derived from sediments and suspended particles using EEM-PARAFAC combined with two-dimensional fluorescence/FTIR correlation analyses, Chemosphere, 219, 45-53, http://dx.doi.org/10.1016/S1352-2310(02)00654-4, 2019.

Huang, R. J., Yang, L., Cao, J., Chen, Y., Chen, Q., Li, Y., Duan, J., Zhu, C., Dai, W., Wang, K., Lin, C., Ni, H., Corbin, J. C., Wu, Y., Zhang, R., Tie, X., Hoffmann, T., O'Dowd, C., and Dusek, U.: Brown carbon aerosol in urban Xi'an, Northwest

China: The composition and light absorption properties, Environ. Sci. Technol., 52, 6825–6833, http://dx.doi.org/10.1021/acs.est.8b02386, 2018.

Huo, S., Xi, B., Yu, H., He, L., and Fan, S.: Characteristics of dissolved organic matter(DOM) in leachate with different landfill ages, J. Environ. Sci, 20, 492–498, http://dx.doi.org/10.1016/S1001-0742(08)62085-9, 2008.

Jane, S. F., Winslow, L. A., Remucal, C. K., and Rose, K. C.: Long-term trends and synchrony in dissolved organic matter characteristics in Wisconsin, USA, lakes: Quality, not quantity, is highly sensitive to climate, J. Geophys. Res. Biogeosci., 122, 546–561, http://dx.doi.org/10.1002/2016JG003630, 2017.

Jang, K. S., Choi, A. Y., Choi, M., Kang, H., Kim, T. W., and Park, K. T.: Size-segregated chemical compositions of HULISs in ambient aerosols collected during the winter season in Songdo, South Korea, Atmosphere., 10, 226, http://dx.doi.org/doi:10.3390/atmos10040226, 2019.

Kim, H., Kim, J. Y., Jin, H. C., Lee, J. Y., and Lee, S. P.: Seasonal variations in the light-absorbing properties of water-soluble and insoluble organic aerosols in Seoul, Korea, Atmos. Environ., 129, 234–242, http://dx.doi.org/10.1016/j.atmosenv.2016.01.042, 2016.

Korshin, G. V., Li, C. W., and Benjamin, M. M.: The decrease of UV absorbance as an indicator of TOX formation, Water Res., 31, 946–949, http://dx.doi.org/10.1016/S0043-1354(96)00393-4, 1997.

Kroflič, A., Frka, S., Simmel, M., Wex, H., and Grgić, I.: Size-resolved surface-active substances of atmospheric aerosol: Reconsideration of the impact on cloud droplet formation, Environ. Sci. Technol., 52, 9179–9187, http://dx.doi.org/10.1021/acs.est.8b02381, 2018.

Laskin, A., Laskin, J., and Nizkorodov, S. A.: Chemistry of atmospheric brown carbon, Chem. Rev., 115, 4335–4382, http://dx.doi.org/10.1021/cr5006167, 2015.

Lin, J. J. and Lee, L. C.: Characterization of n-alkanes in urban submicron aerosol particles (PM_1), Atmos. Environ., 38, 2983–2991, http://dx.doi.org/10.1016/j.atmosenv.2004.02.048, 2004.

Lin, P., Aiona, P. K., Li, Y., Shiraiwa, M., Laskin, J., Nizkorodov, S. A., and Laskin, A.: Molecular characterization of brown carbon in biomass burning aerosol particles, Environ. Sci. Technol., 50, 11815–11824, http://dx.doi.org/10.1021/acs.est.6b03024, 2016.

Liu, J., Bergin, M., Guo, H., King, L., Kotra, N., Edgerton, E., and Weber, R. J.: Size-resolved measurements of brown carbon in water and methanol extracts and estimates of their contribution to ambient fine-particle light absorption, Atmos. Chem. Phys., 13, 12389-12404, http://dx.doi.org/10.5194/acp-13-12389-2013, 2013.

Liu, S., Benedetti, M. F., Han, W., and Korshin, G. V.: Comparison of the properties of standard soil and aquatic fulvic and humic acids based on the data of differential absorbance and fluorescence spectroscopy, Chemosphere, 261, 128189, http://dx.doi.org/10.1016/j.chemosphere.2020.128189, 2020.

Mo, Y., Li, J., Liu, J., Zhong, G., Cheng, Z., Tian, C., Chen, Y., and Zhang, G.: The influence of solvent and pH on determination of the light absorption properties of water-soluble brown carbon, Atmos. Environ., 161, 90–98, http://dx.doi.org/10.1016/j.atmosenv.2017.04.037, 2017.

Mu, S., Wang, S., Liang, S., Xiao, K., Fan, H., Han, B., Liu, C., Wang, X., and Huang, X.: Effect of the relative degree of foulant “hydrophobicity” on membrane fouling, J. Membr. Sci., 570, 1–8, http://dx.doi.org/10.1016/j.memsci.2018.10.023, 2019.

Ni, X., Pan, Y., Shao, P., Tian, S., Zong, Z., Gu, M., Liu, B., Liu, J., Cao, J., and Sun, Q.: Size distribution and formation processes of aerosol water-soluble organic carbon during winter and summer in urban Beijing, Atmos. Environ., 244, 117983, http://dx.doi.org/10.1016/j.atmosenv.2020.117983, 2021.

Pandey, A., Hsu, A., Tiwari, S., Pervez, S., and Chakrabarty, R. K.: Light absorption by organic aerosol emissions rivals that of black carbon from residential biomass fuels in South Asia, Environ. Sci. Technol. Lett., 7, 266–272, http://dx.doi.org/10.1021/acs.estlett.0c00058, 2020.

Park, S., Cho, S. Y., and Bae, M. S.: Source identification of water-soluble organic aerosols at a roadway site using a positive matrix factorization analysis, Sci. Total. Environ., 533, 410-421, http://dx.doi.org/10.1016/j.scitotenv.2015.07.004, 2015.

Phillips, S. M., Bellcross, A. D., and Smith, G. D.: Light absorption by brown carbon in the Southeastern United States is pH-dependent, Environ. Sci. Technol., 51, 6782–6790, http://dx.doi.org/10.1021/acs.est.7b01116, 2017.

Qin, J., Zhang, L., Zhou, X., Duan, J., Mu, S., Xiao, K., Hu, J., and Tan, J.: Fluorescence fingerprinting properties for exploring water-soluble organic compounds in $PM_{2.5}$ in an industrial city of northwest China, Atmos. Environ., 184, 203–211, http://dx.doi.org/10.1016/j.atmosenv.2018.04.049, 2018.

Qin, J., Tan, J., Zhou, X., Yang, Y., Qin, Y., Wang, X., Shi, S., Xiao, K., and Wang, X.: Particle size-dependent fluorescence properties of water-soluble organic compounds (WSOC) and their atmospheric implications on the aging of WSOC, Atmos. Chem. Phys., 1–24, http://dx.doi.org/10.5194/acp-22-465-2022, 2021a.

Qin, Y., Qin, J., Zhou, X., Yang, Y., Chen, R., Tan, J., Xiao, K., and Wang, X.: Effects of pH on light absorption properties of water-soluble organic compounds in particulate matter emitted from typical emission sources, J. Hazard. Mater., 424, 127688, http://dx.doi.org/10.1016/j.jhazmat.2021.127688, 2022.

Qin, Y., Yang, Y., Qin, J., Zhang, L., Guo, S., Zhou, X., Chen, R., Tan, J., Xiao, K., and Wang, X.: pH-responsive fluorescence EEM to titrate the interaction between fluorophores and acid/base groups in water-soluble organic compounds of $PM_{2.5}$, Environ. Sci. Technol. Lett., 8, 108–113, http://dx.doi.org/10.1021/acs.estlett.0c00645, 2021b.

Schendorf, T. M., Del Vecchio, R., Bianca, M., and Blough, N. V.: Combined effects of pH and borohydride reduction on the optical properties of humic substances (HS): A comparison of optical models, Environ. Sci. Technol., 53, 6310–6319, http://dx.doi.org/10.1021/acs.est.9b01516, 2019.

Schulman, S. G., Winefordner, J. D., and Kolthoff, I. M.: Molecular luminescence spectroscopy : methods and applications, Wiley,1985.

Shen, Y., Fichot, C. G., and Benner, R.: Floodplain influence on dissolved organic matter composition and export from the Mississippi—Atchafalaya River system to the Gulf of Mexico, Limnol. Oceanogr., 57, 1149–1160, http://dx.doi.org/10.4319/lo.2012.57.4.1149, 2012.

Sun, Y., Zhang, Q., Zheng, M., Ding, X., Edgerton, E. S., and Wang, X.: Characterization and source apportionment of water-soluble organic matter in atmospheric fine particles ($PM_{2.5}$) with high-resolution aerosol mass spectrometry and GC–MS, Environ. Sci. Technol., 45, 4854–4861, http://dx.doi.org/10.1021/es200162h, 2011.

Wang, J., Ye, J., Zhang, Q., Zhao, J., Wu, Y., Li, J., Liu, D., Li, W., Zhang, Y., and Wu, C.: Aqueous production of secondary organic aerosol from fossil-fuel emissions in winter Beijing haze, Proc. Natl. Acad. Sci. U.S.A., 118, http://dx.doi.org/10.1073/pnas.2022179118, 2021.

Wang, L., Wang, Y., Li, Y., Zhang, W., Zhang, H., Niu, L., and Habibul, N.: Benthic biofilm bacterial communities and their

linkage with water-soluble organic matter in effluent receivers, Int. J. Environ., 19, 1994, http://dx.doi.org/10.3390/ijerph19041994, 2022.

Wang, X. m. and Waite, T. D.: Role of gelling soluble and colloidal microbial products in membrane fouling, Environ. Sci. Technol., 43, 9341–9347, http://dx.doi.org/10.1021/es9013129, 2009.

Wu, G., Wan, X., Gao, S., Fu, P., Yin, Y., Li, G., Zhang, G., Kang, S., Ram, K., and Cong, Z.: Humic-like substances (HULIS) in aerosols of central Tibetan Plateau (Nam Co, 4730 m asl): Abundance, light absorption properties, and sources, Environ. Sci. Technol., 52, 7203–7211, http://dx.doi.org/10.1021/acs.est.8b01251, 2018.

Wu, J., Zhang, H., He, P. J., and Shao, L. M.: Insight into the heavy metal binding potential of dissolved organic matter in MSW leachate using EEM quenching combined with PARAFAC analysis, Water Res., 45, 1711–1719, http://dx.doi.org/10.1016/j.watres.2010.11.022, 2011.

Xiao, K., Shen, Y.-X., Liang, S., Liang, P., Wang, X.-M., and Huang, X.: A systematic analysis of fouling evolution and irreversibility behaviors of MBR supernatant hydrophilic/hydrophobic fractions during microfiltration, J. Membr. Sci., 467, 206–216, http://dx.doi.org/10.1016/j.memsci.2014.05.030, 2014.

Xiao, K., Liang, S., Xiao, A., Lei, T., Tan, J., Wang, X., and Huang, X.: Fluorescence quotient of excitation–emission matrices as a potential indicator of organic matter behavior in membrane bioreactors, Environ. Sci. Water Res. Technol., 4, 281–290, http://dx.doi.org/10.1039/C7EW00270J, 2018a.

Xiao, K., Han, B., Sun, J., Tan, J., Yu, J., Liang, S., Shen, Y., and Huang, X.: Stokes shift and specific fluorescence as potential indicators of organic matter hydrophobicity and molecular weight in membrane bioreactors, Environ. Sci. Technol., 53, 8985–8993, http://dx.doi.org/10.1021/acs.est.9b02114, 2019.

Xiao, K., Yu, J., Wang, S., Du, J., Tan, J., Xue, K., Wang, Y., and Huang, X.: Relationship between fluorescence excitation-emission matrix properties and the relative degree of DOM hydrophobicity in wastewater treatment effluents, Chemosphere., 254, 126830, http://dx.doi.org/10.1016/j.chemosphere.2020.126830, 2020.

Xiao, K., Shen, Y., Sun, J., Liang, S., Fan, H., Tan, J., Wang, X., Huang, X., and Waite, T. D.: Correlating fluorescence spectral properties with DOM molecular weight and size distribution in wastewater treatment systems, Environ. Sci. Water Res. Technol., 4, 1933−1943, http://dx.doi.org/10.1039/C8EW00504D, 2018b.

Xie, Q., Su, S., Chen, S., Zhang, Q., Yue, S., Zhao, W., Du, H., Ren, H., Wei, L., and Cao, D.: Molecular characterization of size-segregated organic aerosols in the urban boundary layer in wintertime Beijing by FT-ICR MS, Faraday Discuss., 226, 457–478, http://dx.doi.org/10.1039/D0FD00084A, 2021.

Young, T. R., Li, W., Guo, A., Korshin, G. V., and Dodd, M. C.: Characterization of disinfection byproduct formation and associated changes to dissolved organic matter during solar photolysis of free available chlorine, Water Res., 146, 318–327, http://dx.doi.org/10.1016/j.watres.2018.09.022, 2018.

Yu, J., Yu, G.-H., Park, S., and Bae, M.-S.: Chemical and absorption characteristics of water-soluble organic carbon and humic-like substances in size-segregated particles from biomass burning emissions, Asian J. Atmospheric Environ., 11, 96–106, http://dx.doi.org/10.5572/ajae.2017.11.2.096, 2017.

Zhang, L., Luo, Z., Xiong, R., Liu, X., Li, Y., Du, W., Chen, Y., Pan, B., Cheng, H., and Shen, G.: Mass absorption efficiency of black carbon from residential solid fuel combustion and its association with carbonaceous fractions, Environ. Sci. Technol., 55, 10662–10671, http://dx.doi.org/10.1021/acs.est.1c02689, 2021.

https://doi.org/10.5194/acp-2022-321
Preprint. Discussion started: 18 May 2022

Atmospheric Chemistry and Physics Discussions

Zhang, Y., Wei, D., Huang, R., Yang, M., Zhang, S., Dou, X., Wang, D., and Vimonses, V.: Binding mechanisms and QSAR
555 modeling of aromatic pollutant biosorption on Penicillium oxalicum biomass, Chem. Eng. J., 166, 624–630,
http://dx.doi.org/10.1016/j.cej.2010.11.034, 2011.